Superexchanges and Charge Transfer in $La_3Ni_2O_7$ Thin Films

Yuxun Zhong(钟宇勋), Wéi Wú(吴为)*, and Dao-Xin Yao(姚道新)*

State Key Laboratory of Optoelectronic Materials and Technologies, Guangdong Provincial Key Laboratory of Magnetoelectric Physics and Devices, Institute of Neutron Science and Technology, School of Physics, Sun Yat-Sen University, Guangzhou 510275, China

(Received 2 December 2025; accepted manuscript online 10 February 2026)

The recent discovery of ambient-pressure superconductivity with a critical temperature T_c exceeding 40 K in $La_3Ni_2O_7$ thin films represents a significant advancement in the field of nickelate superconductivity. Motivated by recent experimental reports, we investigate an 11-band d–p Hubbard model with tight-binding parameters derived from *ab initio* calculations, employing large-scale determinant quantum Monte Carlo and cellular dynamical mean-field theory. Our results show that the dominant superexchange couplings in the $La_3Ni_2O_7$ thin films are substantially weaker than those in the bulk material at 29.5 GPa. Specifically, the out-of-plane antiferromagnetic correlation between the Ni-$d_{3z^2-r^2}$ orbitals is reduced by approximately 27% in the film, whereas the in-plane magnetic correlations remain largely unaffected. We further evaluate the corresponding antiferromagnetic coupling constants, $J_\perp$ and $J_\parallel$, within a perturbative framework. Regarding charge-transfer properties, we find that biaxial compressive strain in the films reduces the charge-transfer gap. We further resolve the orbital distribution of doped holes and electrons between the IP (Ni-$d_{x^2-y^2}$ and O-p_x/p_y) and OP (Ni-$d_{3z^2-r^2}$ and O-p_z) orbitals, revealing a pronounced particle–hole asymmetry. These findings lay the groundwork for constructing a low-energy t–J model for $La_3Ni_2O_7$ films and provide key insights into the physical distinctions between thin-film and bulk bilayer nickelates.

DOI: 10.1088/0256-307X/43/3/030713 CSTR: 32039.14.0256-307X.43.3.030713

Introduction. The discovery of pressure-induced superconductivity in Ruddlesden–Popper (RP) nickelates, first in bilayer $La_3Ni_2O_7$ ($T_c \approx 80$ K)[1] and subsequently in trilayer $La_4Ni_3O_{10}$ ($T_c = 20$–30 K),[2,3] has prompted extensive research. After numerous theoretical investigations[4–35] and experimental studies,[3,36–42] various protocols have been proposed to realize superconductivity without external pressure, including both chemical substitution[43–46] and strain engineering.[47–50] Recent experiments have achieved this goal for thin films of $La_3Ni_2O_7$ (LNO)[51] and $(La,Pr)_3Ni_2O_7$,[52] reporting superconductivity at ambient pressure with T_c exceeding 40 K. This advance overcomes the experimental difficulties associated with high-pressure measurements, facilitating the use of sophisticated probes, such as angle-resolved photoemission spectroscopy and scanning tunneling microscopy.

The superconductivity observed in these experiments is achieved by growing LNO films on substrates with reduced lattice constants (such as $LaAlO_3$ or $SrLaAlO_4$), which impose a strong in-plane biaxial compressive strain.[53] This strain suppresses octahedral tilting in the *Amam* phase of bulk materials at ambient pressure,[47,54,55] stabilizing a tetragonal structure in the films that is analogous to the high-pressure $Fmmm$ or $I4/mmm$ phase of superconducting bulk materials. Given this structural similarity, the low-energy physics is often assumed to be comparable between high-pressure bulk materials and ambient-pressure films. Yet, whether their effective Hamiltonians are truly equivalent is untested. A central unresolved issue, therefore, is to what extent the modified lattice parameters in the films alter the strength of magnetic superexchange couplings and the orbital distribution of the charge carriers. These two factors are believed to govern the system's superconducting properties.

To address this issue, we investigate an 11-band d–p Hubbard model that includes four $3d_{x^2-y^2}/3d_{3z^2-r^2}$ orbitals of nickel and seven most relevant 2p orbitals of oxygen in the NiO_2 bilayer per unit cell.[56] We perform numerically exact determinant quantum Monte Carlo (DQMC) simulations[57,58] and cellular dynamical mean-field theory (CDMFT) calculations[59,60] in the normal state of the system. Our results suggest that the LNO thin-film system exhibits weaker interlayer (IT) antiferromagnetic (AFM) couplings between $d_{3z^2-r^2}$ orbitals, whereas the intra-layer (IR) AFM couplings between $d_{x^2-y^2}$ orbitals remain nearly unchanged compared with bulk LNO. Furthermore, we analyze the charge-transfer properties[61] within the Zaanen–Sawatzky–Allen (ZSA) framework,[62] which has been shown to be crucial for understanding T_c in cuprate superconductors.[63–67] We find that holes introduced via heterovalent doping are distributed approximately evenly between in-plane (IP) and out-of-plane (OP) orbitals, whereas electron doping favors an occupancy ratio of roughly 3:1. By comparing with the experimental doping phase diagram[68] of superconducting $La_{3-x}Sr_xNi_2O_7$ films, we argue that the occupation

*Corresponding authors. Email: wuwei69@mail.sysu.edu.cn; yaodaox@mail.sysu.edu.cn
© 2026 Chinese Physical Society and IOP Publishing Ltd. All rights, including for text and data mining, AI training, and similar technologies, are reserved.

number of the $d_{3z^2-r^2}$ orbital is crucial for determining the type of superconductivity,[69] namely, whether it is driven by Hund's coupling J_H [19–21,70] or governed by hybridization V between e_g orbitals.[30,71,72]

Model and Method. To investigate the superexchange couplings and charge-transfer properties of the LNO thin films, we consider a high-energy effective model including eleven Ni-d and O-p orbitals. The Hamiltonian is given by

$$\begin{aligned} H = & \sum_{ijab\alpha\beta\sigma} t_{ia\alpha,jb\beta} c^{\dagger}_{ia\alpha\sigma} c_{jb\beta\sigma} + \sum_{a\alpha\sigma} (\varepsilon_{a\alpha} - \mu) n_{a\alpha\sigma} \\ & - \sum_{ia\alpha\sigma} E^{a\alpha}_{\mathrm{DC}} n^{\mathrm{d}}_{ia\alpha\sigma} + U \sum_{ia\alpha} n^{\mathrm{d}}_{ia\alpha\uparrow} n^{\mathrm{d}}_{ia\alpha\downarrow} \\ & + \sum_{iab\alpha\beta\sigma\sigma'} (V - J_{\mathrm{H}}\delta_{\sigma\sigma'}) n^{\mathrm{d}}_{ia\alpha\sigma} n^{\mathrm{d}}_{jb\beta\sigma'}, \end{aligned} \tag{1}$$

where i/j, a/b, and α/β denote lattice sites, NiO_2 layers, and orbitals, respectively. The index σ denotes the spin degree of freedom. The superscript d indicates that the Hubbard interaction U is applied only to the Ni-3d orbitals. Here, $t_{ijab\alpha\beta}$ represents the electron hopping integral, and $\varepsilon_{a\alpha}$ denotes the on-site energy of orbital α in layer a. U is the Hubbard repulsion between two electrons on the same d orbital, and $V = U - 2J_{\mathrm{H}}$ is for that on two different orbitals,[73] where J_{H} is the Ising-type Hund's coupling.[15] The pair-hopping and spin-flip terms in Hund's coupling are neglected. For given value of J_{H}, retaining only the Ising-type component of Hund's coupling will in general enhances its overall compared to including all terms of the full Hund's coupling. The double-counting term E_{DC} is subtracted in both the DQMC and CDMFT calculations. We adopt Held's formula [Eqs. (36) and (45) of Ref. [74]] for the double-counting, $E_{\mathrm{DC}} = \frac{1}{3}(U + 2V - J_{\mathrm{H}})(n^0_{\mathrm{d}} - 0.5)$, where n^0_{d} is the occupation number of the d orbitals in the non-interacting limit. In this case, $n^0_{\mathrm{d}} \approx 2.14$. The hopping parameters and on-site energies are adopted from the DFT calculations on the double-stacked LNO thin film reported in Ref. [56]. See also Fig. 1(a) and its caption for all the hopping parameters and on-site energies. Based on these DFT results,[56] we set the chemical potential $\mu = 0$ in the Hamiltonian to represent pristine LNO thin films at ambient pressure. To explore different doping regimes, we vary μ and define the hole concentration as $n_{\mathrm{h}} = \frac{1}{4}(22 - \sum_{a\alpha\sigma} n_{a\alpha\sigma})$, which corresponds to the average number of holes per d orbital per site. Unless stated otherwise, we use $U = 7\,\mathrm{eV}$ as the default parameters[15,61] for the Ni e_g orbitals. For comparison with bulk LNO, we employ a separate parameter set for the corresponding 11-band model.[4,15] We perform calculations on a two-dimensional square lattice containing up to $6\times6\times11 = 396$ orbitals in the DQMC simulations and on an effective impurity cluster with $2 \times 2 \times 11 = 44$ orbitals in the CDMFT calculations, as illustrated in Fig. 1(b). Due to the fermionic sign problem in DQMC, the simulations are restricted to a high temperature regime. The lowest temperature reached is $T = 0.25$ (in eV units), with an average sign $\langle s \rangle \approx 0.79$. CDMFT is employed as a complementary approach to access lower temperatures, where values down to $T \sim 0.08$ can be achieved while maintaining an average sign of $\langle s \rangle \approx 0.56$ in the impurity solver.

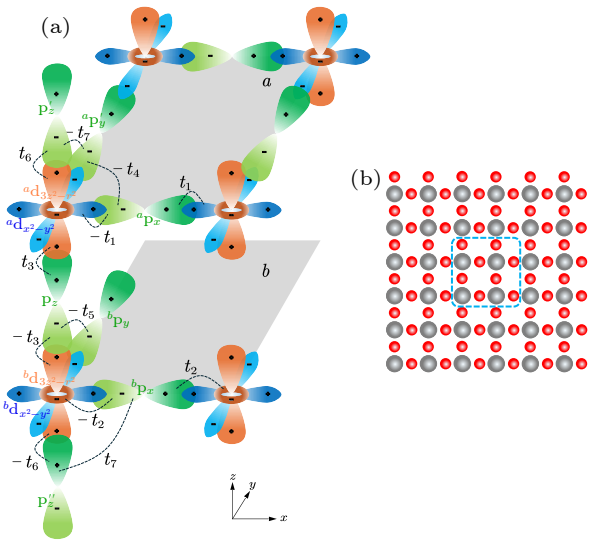

Fig. 1. Schematic of the 11-band bilayer LNO thin-film lattice model with seven major hopping parameters and the illustration of the two-dimensional NiO_2 lattice for DQMC and CDMFT simulations. (a) The orange, blue, and green electron clouds denote Ni-3$d_{3z^2-r^2}$, Ni-3$d_{x^2-y^2}$ and O-2p orbitals, respectively. For brevity, some orbitals on plane b are not displayed. Four hopping processes between Ni-d and O-p orbitals predominantly contribute to the superexchange interactions between neighboring Ni-d orbitals: $t_1 = -1.4795$, $t_2 = 0.6605$, $t_3 = -1.4565$, $t_6 = 1.2045$. The site energies are $\varepsilon_{\mathrm{d}_{x^2-y^2}} = -0.962$, $\varepsilon_{\mathrm{d}_{3z^2-r^2}} = -1.070$, $\varepsilon_{\mathrm{p}x/\mathrm{p}y} = -4.650$, $\varepsilon_{\mathrm{p}_z} = -4.078$, $\varepsilon_{\mathrm{p}_z'} = \varepsilon_{\mathrm{p}_z''} = -2.977$.[56] The superexchange interactions between the IR $d_{x^2-y^2}$ and $d_{3z^2-r^2}$ orbitals (not shown here) vanish due to symmetry. Here $t_4 = 0.5675$, $t_5 = 0.4315$, $t_7 = 0.4115$ denote electron hopping processes between O-p orbitals. (b) Dark spheres denote the positions of Ni, while light spheres represent the positions of O in the NiO_2 plane. The 6×6 unit cells used in DQMC simulations are shown, whereas the 2×2 CDMFT effective cluster is outlined by a blue dashed rectangle. For clarity, only one NiO_2 layer is shown.

Superexchanges. First, we discuss the magnetic exchange couplings in LNO thin films and compare them with those in bulk LNO. As shown in Fig. 1(a), four hopping processes (t_1, t_2, t_3, and t_6) contribute dominantly to the superexchange interactions, yielding estimated coupling constants of $J_{\parallel} \sim 0.095\,\mathrm{eV}$ and $J_{\perp} \sim 0.127\,\mathrm{eV}$ at $U = 7\,\mathrm{eV}$ in the atomic limit (see Table 1). In the atomic limit, the charge-transfer picture for spin-1/2 electron system suggests that the energy difference between the spin singlet and spin triplet states composed of the two Ni-d orbitals can be expressed as

$$\begin{aligned} J &= E_{\uparrow\uparrow} - E_{\uparrow\downarrow} \\ &= 2|t_{\mathrm{pd}_1} t_{\mathrm{pd}_2}|^2 \Big[\frac{1}{U + \Delta_{\mathrm{pd}_2} - \Delta_{\mathrm{pd}_1}} \Big(\frac{1}{U + \Delta_{\mathrm{pd}_1}} \Big)^2 \\ &\quad + \frac{1}{U + \Delta_{\mathrm{pd}_1} - \Delta_{\mathrm{pd}_2}} \Big(\frac{1}{U + \Delta_{\mathrm{pd}_2}} \Big)^2 \\ &\quad + \frac{1}{2U + \Delta_{\mathrm{pd}_1} + \Delta_{\mathrm{pd}_2}} \Big(\frac{1}{U + \Delta_{\mathrm{pd}_1}} + \frac{1}{U + \Delta_{\mathrm{pd}_2}} \Big)^2 \Big], \end{aligned} \tag{2}$$

where $t_{\mathrm{pd}_{1,2}}$ denotes hopping between the Ni-$d_{1,2}$ and O-p orbitals. The energy difference between the lower Hubbard band of the Ni-d orbitals and the O-p orbital is given

by $\Delta_{\mathrm{pd}_{1,2}} = \varepsilon_{\mathrm{d}_{1,2}} - \varepsilon_{\mathrm{p}}$, with the double-counting term included in $\varepsilon_{\mathrm{d}_{1,2}}$. Equation 2 represents the second-order approximation result from perturbation theory, which describes the superexchange between two neighboring Ni-3d orbitals in the atomic limit. We compute the IR ($J_\parallel$) and IT ($J_\perp$) superexchange couplings within a separate-channel approximation, where $J_\parallel$ is derived from the $\mathrm{d}_{x^2-y^2}-\mathrm{p}_{x/y}-\mathrm{d}_{x^2-y^2}$ hopping pathway, and $J_\perp$ originates from the $\mathrm{d}_{3z^2-r^2}-\mathrm{p}_z-\mathrm{d}_{3z^2-r^2}$ channel. Our results for J at various U values are summarized in Table 1, where the AFM coupling strength J decreases monotonically with increasing U. For example, the interlayer coupling $J_\perp$ decreases from 0.320 eV at $U = 3$ eV to 0.127 eV at $U = 7$ eV.

In DQMC calculations, the magnetic correlation functions can be exactly measured at high temperatures. Figures 2(a) and 2(b) show the magnitudes of the spin correlation function $\langle S_{ia\alpha} \cdot S_{jb\beta}\rangle$ between neighboring d orbitals at $T = 0.25$ and half filling from DQMC, and at $\mu = 0$ and $T = 0.125$ from CDMFT, respectively. Here, $S_{ia\alpha}$ is a spin operator with site index i, layer a, and orbital α. These results depict the relative strengths of the major exchange couplings in LNO thin films. At $T = 0.25$ and half-filling, similar to bulk LNO, the dominant AFM exchange coupling in the films is the IT $\mathrm{d}_{3z^2-r^2} - \mathrm{d}_{3z^2-r^2}$ channel,

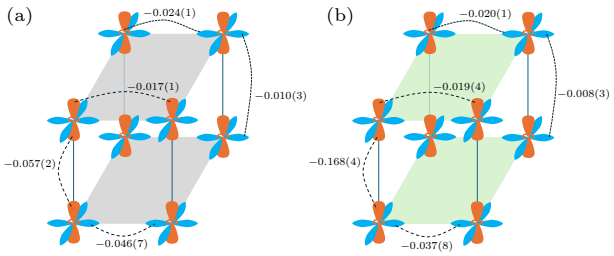

Fig. 2. The spin–spin correlation function $\langle S_{ia\alpha} \cdot S_{jb\beta}\rangle$ for four neighboring d orbitals is shown numerically to illustrate the relative strength of the AFM superexchange couplings in the system. The orange and blue symbols represent the $\mathrm{d}_{3z^2-r^2}$ and $\mathrm{d}_{x^2-y^2}$ orbitals, respectively. We use the specific values $U = 7$ and $J_\mathrm{H} = 0.15U$, consistent with values obtained from constrained RPA.[14] (a) shows results from DQMC at half filling ($n_\mathrm{h} = 1$, $\mu = 1.5$) and $T = 0.25$ eV, and (b) shows results from CDMFT at $\mu = 0$ ($n_\mathrm{h} \approx 1.234$). Note that the on-site IT magnetic correlations between the $\mathrm{d}_{x^2-y^2}$ and $\mathrm{d}_{3z^2-r^2}$ orbitals, arising from Hund's coupling, are not shown.

Table 1. Superexchange couplings J obtained from Eq. (2) for various values of the Hubbard interaction U. The vertical IT AFM coupling $J_\perp$, IR AFM coupling $J_\parallel$, and their ratio $J_\parallel/J_\perp$ are listed. The double counting correction applied here is the same as those in the DQMC and CDMFT simulations: $E_\mathrm{DC} = (n^0_{\mathrm{d}\alpha} - 0.5)U = 0.571U$ for both $\mathrm{d}_{x^2-y^2}$ and $\mathrm{d}_{3z^2-r^2}$ orbitals. All calculations are carried out to sixth-order accuracy by using perturbation theory.

U/eV	$J_\perp$/eV	$J_\parallel$/eV	$J_\parallel/J_\perp$
3	0.320	0.257	80.3%
4	0.256	0.196	76.6%
5	0.200	0.151	75.7%
6	0.158	0.119	75.6%
7	0.127	0.095	75.6%
8	0.103	0.078	75.7%
9	0.085	0.064	75.9%

with a value of $\langle S \cdot S\rangle = -0.057(2)$. The next strongest AFM exchange comes from IR nearest-neighbor (NN) $\mathrm{d}_{x^2-y^2} - d_{x^2-y^2}$ orbitals, with $\langle S \cdot S\rangle = -0.046(7)$. Compared with bulk LNO, the importance of IP couplings is significantly enhanced in thin films, reaching 81% of the AFM exchange between the IT $\mathrm{d}_{3z^2-r^2} - \mathrm{d}_{3z^2-r^2}$ orbitals. The corresponding ratio for bulk LNO is approximately 60%.[15] The strengths of the IR NN $\mathrm{d}_{x^2-y^2} - \mathrm{d}_{3z^2-r^2}$ and IT $\mathrm{d}_{3z^2-r^2} - \mathrm{d}_{3z^2-r^2}$ AFM correlations are $\langle S \cdot S\rangle = -0.024(1)$ and $\langle S \cdot S\rangle = -0.017(1)$, respectively. These couplings are relatively small due to weak hopping between $\mathrm{d}_{3z^2-r^2}$ and $\mathrm{p}_x/\mathrm{p}_y$ orbitals. Notably, the IT $\mathrm{d}_{x^2-y^2} - \mathrm{d}_{x^2-y^2}$ exchange coupling within a unit cell is the weakest among these magnetic channels. In Fig. 2(b), CDMFT results at $T = 0.125$ and $\mu = 0$ likewise suggest that the IT $\mathrm{d}_{3z^2-r^2} - \mathrm{d}_{3z^2-r^2}$ coupling remains predominant, with $\langle S \cdot S\rangle = -0.168(4)$. Notably, in CDMFT at $\mu = 0$, the correlation between IT $\mathrm{d}_{x^2-y^2} - \mathrm{d}_{x^2-y^2}$ orbitals is again the weakest among the five magnetic couplings. In summary, the IT $\mathrm{d}_{3z^2-r^2} - \mathrm{d}_{3z^2-r^2}$ magnetic correlation dominates over a range of chemical potentials μ (or fillings), suggesting that the $\mathrm{d}_{3z^2-r^2}$ orbitals play a central role in the correlation-driven superconductivity.

Figure 3 presents the temperature dependence of AFM correlations $\langle S_{ia\alpha} \cdot S_{jb\beta}\rangle$ obtained from DQMC simulations at $\mu = 0$. The bulk LNO system exhibits stronger AFM correlations than the thin film for both IR and IT components. This overall suppression of magnetic coupling provides a plausible explanation for the reduced superconducting transition temperature T_c in the thin films.[72] A key distinction in the suppression of magnetic couplings should be emphasized: the reduction of magnetic correlations for the IT $\mathrm{d}_{3z^2-r^2} - \mathrm{d}_{3z^2-r^2}$ component is much more prominent than that for the IR NN $\mathrm{d}_{x^2-y^2} - \mathrm{d}_{x^2-y^2}$ component. The latter is almost identical between the film and bulk systems. Furthermore, the IT $\mathrm{d}_{3z^2-r^2} - \mathrm{d}_{3z^2-r^2}$ magnetic correlation in thin films is not significantly stronger than the IR NN $\mathrm{d}_{x^2-y^2} - \mathrm{d}_{x^2-y^2}$ component. This contrasts sharply with the bulk case, in which the IT $\mathrm{d}_{3z^2-r^2} - \mathrm{d}_{3z^2-r^2}$ correlation is much stronger than its IR $\mathrm{d}_{x^2-y^2} - \mathrm{d}_{x^2-y^2}$ counterpart.[15] These results suggest that both IT $\mathrm{d}_{3z^2-r^2} - \mathrm{d}_{3z^2-r^2}$ and

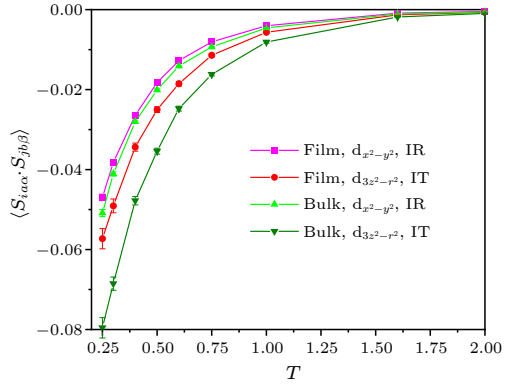

Fig. 3. $\langle S_{ia\alpha} \cdot S_{jb\beta}\rangle$ between pairs of NN d orbitals as a function of temperature T in the pristine system, as obtained from DQMC simulations. The squares indicate IR $\mathrm{d}_{x^2-y^2} - \mathrm{d}_{x^2-y^2}$ correlations, while the circles denote IT $\mathrm{d}_{3z^2-r^2} - \mathrm{d}_{3z^2-r^2}$ correlations.

IR $d_{x^2-y^2} - d_{x^2-y^2}$ components of AFM correlations may play crucial roles in the ambient-pressure superconductivity observed in LNO thin films.

Charge Transfer Properties. Next, we examine the charge-transfer properties of the 11-band Hubbard model. Figure 4 illustrates the evolution of hole/electron concentrations across different orbitals as functions of chemical potentials μ and Hund's coupling J_H. In Fig. 4(a), the hole concentration n_h is shown as a function of μ, where an inflection point near $n_h = 1$ ($\mu_h \sim -1.55$) with a strongly reduced compressibility ($\partial n_h/\partial \mu_h$) suggests the opening of a charge gap at half filling ($n_h = 1$). For the temperatures we have assessed ($T > 0.125$), the $\mu - n_h$ curve is not completely flat, indicating that the charge gap was not fully open. Notably, the reduced flatness of the $\mu - n_h$ curve around $n_h = 1$ for the film (compared with the bulk at this temperature[15]) should point to a smaller charge-transfer gap in the system.

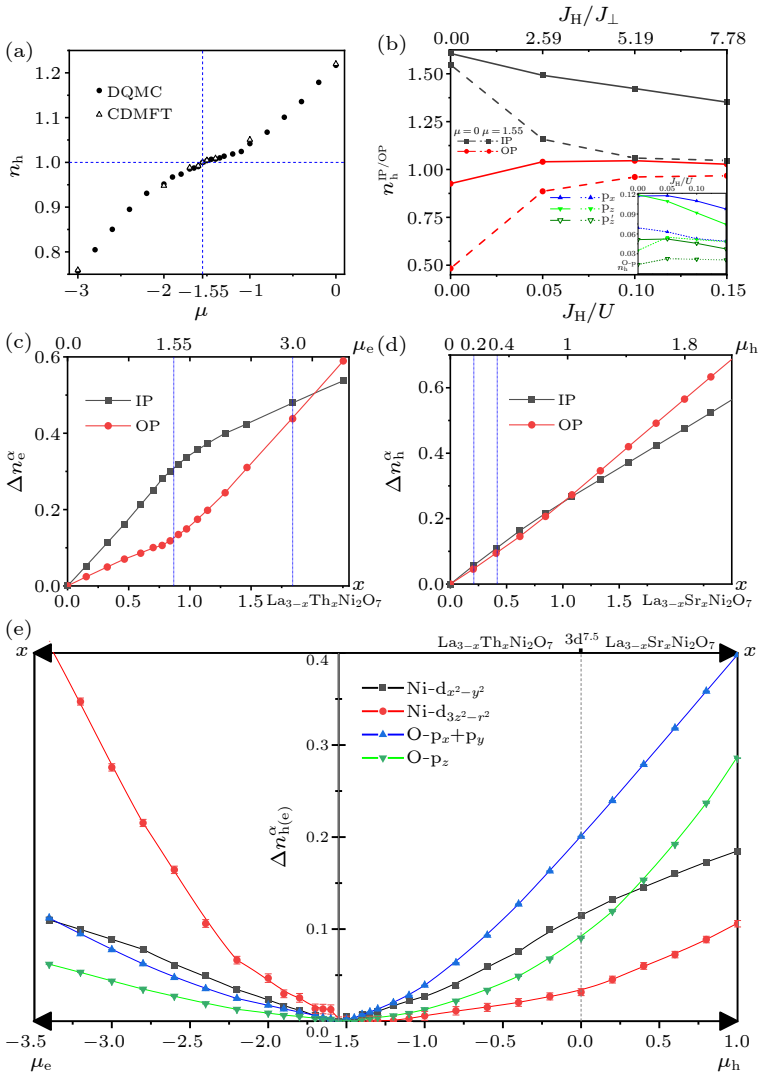

Fig. 4. Charge transfer properties and charge carrier evolution of $La_3Ni_2O_7$ thin films. (a) DQMC and CDMFT results of hole concentration n_h as a function of hole chemical potential μ_h. An inflection point suggests the opening of a charge-transfer gap at half filling when $\mu_h \sim -1.55$. Here $T = 0.3$. (b) Carrier concentrations as functions of Hund's coupling J_H for each orbital in the LNO thin film under half filling (dashed lines) and pristine configuration ($\mu = 0$, solid lines) conditions from CDMFT at $T = 0.125$. The gray and red color curves represent the IP and OP hole concentrations, respectively, while the inset provides more details about the hole concentration on O orbitals. (c) and (d) show electron (hole) concentration variations $\Delta n^\alpha_{e(h)}$ as functions of chemical potential $\mu_{e(h)}$ and $Sr^{2+}(Th^{4+})$ nominal doping level x, respectively. Here, $\Delta n_h^{IP} = \Delta n_h^{d_{x^2-y^2}} + \Delta n_h^{p_x} + \Delta n_h^{p_y}$ denotes the number of holes in the IP $d_{x^2-y^2}$ orbital and p_x/p_y orbitals combined, while $\Delta n_h^{OP} = \Delta n_h^{d_{3z^2-r^2}} + 0.5(\Delta n_h^{p_z} + \Delta n_h^{p'_z})$ denotes the number of holes in the OP orbitals. Note that Δn_h^α represents the difference in hole concentration relative to the pristine LNO thin film (Ni-$3d^{7.5}$), i.e. hole concentration variation $\Delta n_h^\alpha \equiv n_h(\mu) - n_h(\mu_h = 0)$. When Sr doping level $x = 0.203$, the nominal hole content in $La_{3-x}Sr_xNi_2O_7$ corresponds to $\mu_h = 0.2$, while for $\mu_h = 0.4$, the equivalent Sr doping level is $x = 0.406$. At this doping level, superconductivity is no longer observed.[68] (e) The electron concentration variation Δn_e^α as a function of the electron chemical potential μ_e in the regime $\mu_e > 1.55$ (corresponding to electron doping with $n_e > 1$) and hole concentration variation Δn_h^α in the regime of hole doping, where $n_h = 2 - n_e > 1$ ($n_{e/h} = \sum_{a,\alpha} n_{e/h}^{a\alpha}$), respectively. Here, α denotes distinct α orbitals and charge concentration variation $\Delta n_{e/h}^\alpha \equiv n_{e/h}(\mu) - n_{e/h}(\mu_e = 1.55)$. Results in (c), (d), and (e) above are from DQMC simulations at $T = 0.3$.

Figure 4(e) presents the orbital-resolved distribution of doped charge carriers. As the hole chemical potential $\mu_{\rm h} \equiv -\mu$ or electron chemical potential $\mu_{\rm e} \equiv \mu$ is tuned away from half filling, the doped carriers enter different orbitals. Specifically, doped holes predominantly occupy the O-p orbitals [blue and green lines in the right panel of Fig. 4(e)], whereas the doped electrons primarily occupy the Ni-d orbitals [red and black curves in the left panel of Fig. 4(e)]. This observation confirms the charge-transfer nature of the correlated states in the system.[62,63] Moreover, we observed that the $d_{x^2-y^2}$ orbital contains a higher concentration of doped holes than the $d_{3z^2-r^2}$ orbital in the case of hole doping ($\mu_{\rm h} > -1.55$). This suggests that the $d_{3z^2-r^2}$ orbitals are more correlated than the $d_{x^2-y^2}$ orbitals under hole doping.

To shed light on low-energy effective models integrating the degrees of freedom of O, we grouped the Ni-3d and O-2p orbitals into two categories: (i) OP correlated orbitals, including $d_{3z^2-r^2}$, p_z and p'_z and (ii) IP correlated orbitals comprising $d_{x^2-y^2}$ and p_x/p_y orbitals. As shown in Figs. 4(c) and 4(d), the additional holes doped into the LNO films are distributed nearly equally between the IP and OP orbitals. In contrast, for electron doping around $\mu_{\rm e} \sim 0$, the doped carriers favor IP orbitals over OP orbitals at a ratio of approximately 3:1. This stark asymmetry between electron and hole doping (1:1 vs. 3:1) suggests a dopant-type-dependent superconducting phase diagram. This is particularly relevant to experiments in which Sr-doping (Strontium) introduces holes,[68] whereas Th-doping (Thorium) or Hf-doping (Hafnium) introduces electrons.

The data in Fig. 4(e) also show a significant difference in the carrier response; under identical chemical potential changes, the hole variation in LNO films is approximately twofold greater than that in the bulk.[15] This indicates that LNO thin films possess enhanced charge-transfer capabilities and, consequently, a smaller charge-transfer gap Δ.[75] Our conclusion aligns with recent spectroscopic experiments,[76] which propose the existence of two types of Zhang–Rice singlets in LNO films and suggest that the IP charge transfer properties are analogous to those of cuprate superconductors.

Finally, we find that the presence of Hund's coupling $J_{\rm H}$ at half filling strongly in general suppresses orbital polarization and hence tends to stabilize a high-spin $S = 1$ state, as illustrated by the dashed lines in Fig. 4(b), which follow Hund's first law. However, for the pristine configuration ($\mu = 0$), the influence of the $J_{\rm H}$ coupling is significantly weakened. In this case, the holes retain preferential occupation of the IP orbitals, as indicated by the solid lines in Fig. 4(b).

Discussion and Conclusion. The observation of superconductivity in $La_3Ni_2O_7$ thin films at ambient pressure[51,52] has spurred the proposal of several effective interacting models for investigating various physical properties,[53,54,77,78] building on insights from *ab initio* calculations.[49,50,56,77,79] These effective models primarily focus on parameterizing magnetic correlations based on direct exchange couplings between Ni-d orbitals, while neglecting the contribution of the degrees of freedom of oxygen. In this study, the 11-band d–p Hubbard model, which incorporates both Ni-3d and O-2p orbitals, provides a more comprehensive understanding of the relative strengths of superexchange couplings and the distributions of charge carriers in $La_3Ni_2O_7$ thin films. Crucially, we resolved the properties of the IP and OP bands, which exhibit remarkably different hole concentrations ($n_{\rm h}$) and correlation strengths. We found that the IR and IT magnetic coupling strengths are more or less comparable, in sharp contrast to IT-coupling-dominated bulk materials. Furthermore, we observed pronounced asymmetry in the charge distribution upon hole/electron doping. In summary, our unified analysis of both magnetic correlations and charge-transfer properties consistently identified the IT Ni-$d_{3z^2-r^2}$ orbital couplings as the dominant factor determining the pairing nature in bilayer nickelate films. The contribution of the more itinerant Ni-$d_{x^2-y^2}$ orbitals in superconducting or normal state, however, appear more subtle and complex, warranting further dedicated investigations.

Acknowledgements. We thank Zhihui Luo and Wenyuan Qiu for helpful discussions. This work was supported by the National Natural Science Foundation of China (Grant Nos. 12494591, 12494594, and 92565303), the National Key R&D Program of China (Grant No. 2022YFA1402802), the Guangdong Provincial Key Laboratory of Magnetoelectric Physics and Devices (Grant No. 2022B1212010008), the Research Center for Magnetoelectric Physics of Guangdong Province (Grant No. 2024B0303390001), and the Guangdong Provincial Quantum Science Strategic Initiative (Grant No. GDZX2401010).

References

[1] Sun H, Huo M, Hu X, Li J, Liu Z, Han Y, Tang L, Mao Z, Yang P, Wang B, Cheng J, Yao D X, Zhang G M, and Wang M 2023 *Nature* **621** 493
[2] Zhu Y, Peng D, Zhang E, Pan B, Chen X, Chen L, Ren H, Liu F, Hao Y, Li N, Xing Z, Lan F, Han J, Wang J, Jia D, Wo H, Gu Y, Gu Y, Ji L, Wang W, Gou H, Shen Y, Ying T, Chen X, Yang W, Cao H, Zheng C, Zeng Q, Guo J G, and Zhao J 2024 *Nature* **631** 531
[3] Li Q, Zhang Y J, Xiang Z N, Zhang Y, Zhu X, and Wen H H 2024 *Chin. Phys. Lett.* **41** 017401
[4] Luo Z, Hu X, Wang M, Wú W, and Yao D X 2023 *Phys. Rev. Lett.* **131** 126001
[5] Zhang Y, Lin L F, Moreo A, and Dagotto E 2023 *Phys. Rev. B* **108** L180510
[6] Lechermann F, Gondolf J, Bötzel S, and Eremin I M 2023 *Phys. Rev. B* **108** L201121
[7] Shilenko D A and Leonov I V 2023 *Phys. Rev. B* **108** 125105
[8] Chen X, Jiang P, Li J, Zhong Z, and Lu Y 2025 *Phys. Rev.* **B** 014515
[9] Ouyang Z, Gao M, and Lu Z Y 2024 *npj Quantum Mater.* **9** 80
[10] Liu Y B, Mei J W, Ye F, Chen W Q, and Yang F 2023 *Phys. Rev. Lett.* **131** 236002
[11] Heier G, Park K, and Savrasov S Y 2024 *Phys. Rev. B* **9** 104508
[12] Zhang Y, Lin L F, Moreo A, Maier T A, and Dagotto E 2024 *Nat. Commun.* **15** 2470

[13] Zhang Y, Lin L F, Moreo A, Maier T A, and Dagotto E 2024 *Phys. Rev. B* **109** 045151
[14] Christiansson V, Petocchi F, and Werner P 2023 *Phys. Rev. Lett.* **131** 206501
[15] Wú W, Luo Z, Yao D X, and Wang M 2024 *Sci. China Phys. Mech. Astron.* **67** 117402
[16] Tian Y H, Chen Y, Wang J M, He R Q, and Lu Z Y 2024 *Phys. Rev. B* **109** 165154
[17] Ryee S, Witt N, and Wehling T O 2024 *Phys. Rev. Lett.* **133** 096002
[18] Shen Y, Qin M, and Zhang G M 2023 *Chin. Phys. Lett.* **40** 127401
[19] Lu C, Pan Z, Yang F, and Wu C 2024 *Phys. Rev. Lett.* **132** 146002
[20] Oh H and Zhang Y H 2023 *Phys. Rev. B* **108** 174511
[21] Qu X Z, Qu D W, Chen J, Wu C, Yang F, Li W, and Su G 2024 *Phys. Rev. Lett.* **132** 036502
[22] Yang H, Oh H, and Zhang Y H 2024 *Phys. Rev. B* **110** 104517
[23] Liao Z, Chen L, Duan G, Wang Y, Liu C, Yu R, and Si Q 2023 *Phys. Rev. B* **108** 214522
[24] Fan Z, Zhang J F, Zhan B, Lv D, Jiang X Y, Normand B, and Xiang T 2024 *Phys. Rev. B* **110** 024514
[25] Kaneko T, Sakakibara H, Ochi M, and Kuroki K 2024 *Phys. Rev. B* **109** 045154
[26] Luo Z, Lv B, Wang M, Wú W, and Yao D X 2024 *npj Quantum Mater.* **9** 61
[27] Yang Q G, Wang D, and Wang Q H 2023 *Phys. Rev. B* **108** L140505
[28] Sakakibara H, Kitamine N, Ochi M, and Kuroki K 2024 *Phys. Rev. Lett.* **132** 106002
[29] Cao Y and Yang Y F 2024 *Phys. Rev. B* **109** L081105
[30] Yang Y F, Zhang G M, and Zhang F C 2023 *Phys. Rev. B* **108** L201108
[31] Huang J, Wang Z, and Zhou T 2023 *Phys. Rev. B* **108** 174501
[32] Huang J, Wang Z D, and Zhou T 2023 *Phys. Rev. B* **108** 174501
[33] Jiang R, Hou J, Fan Z, Lang Z J, and Ku W 2024 *Phys. Rev. Lett.* **132** 126503
[34] Zhang J X, Zhang H K, You Y Z, and Weng Z Y 2024 *Phys. Rev. Lett.* **133** 126501
[35] Wang M, Wen H H, Wu T, Yao D X, and Xiang T 2024 *Chin. Phys. Lett.* **41** 077402
[36] Yang J, Sun H, Hu X, Xie Y, Miao T, Luo H, Chen H, Liang B, Zhu W, Qu G, Chen C Q, Huo M, Huang Y, Zhang S, Zhang F, Yang F, Wang Z, Peng Q, Mao H, Liu G, Xu Z, Qian T, Yao D X, Wang M, Zhao L, and Zhou X J 2024 *Nat. Commun.* **15** 4373
[37] Zhang Y, Su D, Huang Y *et al.* 2024 *Nat. Phys.* **20** 1269
[38] Hou J, Yang P T, Liu Z Y *et al.* 2023 *Chin. Phys. Lett.* **40** 117302
[39] Fan S, Luo Z, Huo M, Wang Z, Li H, Yang H, Wang M, Yao D X, and Wen H H 2024 *Phys. Rev. B* **110** 134520
[40] Wang G, Wang N N, Shen X L, Hou J, Ma L, Shi L F, Ren Z A, Gu Y D, Ma H M, Yang P T, Liu Z Y, Guo H Z, Sun J P, Zhang G M, Calder S, Yan J Q, Wang B S, Uwatoko Y, and Cheng J G 2024 *Phys. Rev. X* **14** 011040
[41] Liu Z, Huo M, Li J *et al.* 2024 *Nat. Commun.* **15** 7570
[42] Li J, Peng D, Ma P, Zhang H, Xing Z, Huang X, Huang C, Huo M, Hu D, Dong Z, Chen X, Xie T, Dong H, Sun H, Zeng Q, Mao H K, and Wang M 2025 *Natl. Sci. Rev.* **12** nwaf220
[43] Pan Z, Lu C, Yang F, and Wu C 2024 *Chin. Phys. Lett.* **41** 087401
[44] Zhang Y, Lin L F, Moreo A, Maier T A, and Dagotto E 2023 *Phys. Rev. B* **108** 165141
[45] Li F, Xing Z, Peng D, Dou J, Guo N, Ma L, Zhang Y, Wang L, Luo J, Yang J, Zhang J, Chang T, Chen Y S, Cai W, Cheng J, Wang Y, Zeng Z, Zheng Q, Zhou R, Zeng Q, Tao X, and Zhang J 2025 arXiv:2501.14584 [cond-mat.supr-con]
[46] Zhu F H, Wang X Y, Shao T N, Zhao Q, Yang W L, Chen C X, Yan M L, Dou R F, Xiong C M, and Nie J C 2025 *Chin. Phys. Lett.* **42** 067303
[47] Osada M, Terakura C, Kikkawa A, Nakajima M, Chen H Y, Nomura Y, Tokura Y, and Tsukazaki A 2025 *Commun. Phys.* **8** 251
[48] Wang B Y, Zhong Y, Abadi S, Liu Y, Yu Y, Zhang X, Wu Y M, Wang R, Li J, Tarn Y, Ko E K, Thampy V, Hashimoto M, Lu D, Lee Y S, Devereaux T P, Jia C, Hwang H Y, and Shen Z X 2025 arXiv:2504.16372 [cond-mat.supr-con]
[49] Bhatt L, Jiang A Y, Ko E K, Schnitzer N, Pan G A, Segedin D F, Liu Y, Yu Y, Zhao Y F, Morales E A, Brooks C M, Botana A S, Hwang H Y, Mundy J A, Muller D A, and Goodge B H 2025 arXiv:2501.08204 [cond-mat.supr-con]
[50] Liu Y, Ko E K, Tarn Y, Bhatt L, Li J, Thampy V, Goodge B H, Muller D A, Raghu S, Yu Y, and Hwang H Y 2025 *Nat. Mater.* **24** 1221
[51] Ko E K, Yu Y, Liu Y *et al.* 2025 *Nature* **638** 935
[52] Zhou G, Lv W, Wang H *et al.* 2025 *Nature* **640** 641
[53] Shao Z Y, Liu Y B, Liu M, and Yang F 2025 arXiv:2501.10409 [cond-mat.supr-con]
[54] Cao Y H, Jiang K Y, Lu H Y, Wang D, and Wang Q H 2025 arXiv:2507.13694 [cond-mat.supr-con]
[55] Samanta B and Georgescu A B 2025 arXiv:2506.11427 [cond-mat.supr-con]
[56] Hu X, Qiu W, Chen C Q, Luo Z, and Yao D X 2025 arXiv:2503.17223 [cond-mat.supr-con]
[57] Blankenbecler R, Scalapino D J, and Sugar R L 1981 *Phys. Rev. D* **24** 2278
[58] Assaad F and Evertz H 2008 *Computational Many-Particle Physics* p. 277
[59] Georges A, Kotliar G, Krauth W, and Rozenberg M J 1996 *Rev. Mod. Phys.* **68** 13
[60] Maier T, Jarrell M, Pruschke T, and Hettler M H 2005 *Rev. Mod. Phys.* **77** 1027
[61] Karp J, Botana A S, Norman M R, Park H, Zingl M, and Millis A 2020 *Phys. Rev. X* **10** 021061
[62] Zaanen J, Sawatzky G A, and Allen J W 1985 *Phys. Rev. Lett.* **55** 418
[63] Ruan W, Hu C, Zhao J, Cai P, Peng Y, Ye C, Yu R, Li X, Hao Z, Jin C, Zhou X, Weng Z Y, and Wang Y 2016 *Sci. Bull.* **61** 1826
[64] Kowalski N, Dash S S, Sémon P, Sénéchal D, and Tremblay A M 2021 *Proc. Natl. Acad. Sci. U.S.A.* **118** e2106476118
[65] Weber C, Yee C, Haule K, and Kotliar G 2012 *EPL* **100** 37001
[66] O'Mahony S M, RenW, ChenW, Chong Y X, Liu X, Eisaki H, Uchida S, Hamidian M H, and Davis J C S 2022 *Proc. Natl. Acad. Sci. U.S.A.* **119** e2207449119
[67] Rybicki D, Jurkutat M, Reichardt S, Kapusta C, and Haase J 2016 *Nat. Commun.* **7** 11413
[68] Hao B, Wang M, Sun W, Yang Y, Mao Z, Yan S, Sun H, Zhang H, Han L, Gu Z, Zhou J, Ji D, and Nie Y 2025 arXiv:2505.12603 [cond-mat.supr-con]
[69] Mo S, Zheng Y, and Wu W 2025 arXiv:2508.04554 [cond-mat.supr-con]
[70] Bejas M, Wu X, Chakraborty D, Schnyder A P, and Greco A 2025 *Phys. Rev. B* **111** 144514
[71] Zheng Y Y and Wú W 2025 *Phys. Rev. B* **111** 035108
[72] Qin Q and Yang Y F 2023 *Phys. Rev. B* **108** L140504
[73] Held K, Keller G, Eyert V, Vollhardt D, and Anisimov V I 2001 *Phys. Rev. Lett.* **86** 5345
[74] Held K 2007 *Adv. Phys.* **56** 829
[75] Zhong H, Hao B, Wei Y, Zhang Z, Liu R, Huang X, Ni X S, dos Reis Cantarino M, Cao K, Nie Y, Schmitt T, and Lu X 2025 arXiv:2502.03178 [cond-mat.supr-con]
[76] Ren X, Sutarto R, Wu X, Zhang J, Huang H, Xiang T, Hu J, Comin R, Zhou X, and Zhu Z 2025 *Commun. Phys.* **8** 52
[77] Yue C, Miao J J, Huang H, Hua Y, Li P, Li Y, Zhou G, Lv W, Yang Q, Yang F, Sun H, Sun Y J, Lin J, Xue Q K, Chen Z, and Chen W Q 2025 *Natl. Sci. Rev.* **12** nwaf253
[78] Qiu W, Luo Z, Hu X, and Yao D X 2025 arXiv:2506.20727 [cond-mat.supr-con]
[79] Shi H, Huo Z, Li G, Ma H, Cui T, Yao D X, and Duan D 2025 arXiv:2502.04255 [cond-mat.supr-con]